Turkish Computational and Theoretical Chemistry

Turkish Comp Theo Chem (TC&TC)

Volume(Issue): 9(5) – Year: 2025 – Pages: 77-85

e-ISSN: 2602-3237

https://doi.org/10.33435/tcandtc.1716394

Received: 14.06.2025 **Accepted:** 24.06.2025 *Research Article*

MOLECULAR DOCKING ANALYSIS OF SMALL FULLERENE (C20, C22, C24) NANOPARTICLES WITH LUNG (1X2J) AND BREAST (3HY3) CANCER TARGET PROTEINS

Saadet Kaya[1]

Sivas Cumhuriyet University, Faculty of Science, Department of Chemistry, Sivas, 58140, Turkey

Abstract: Nanotechnology-based therapeutic approaches play a crucial role in the development of next-generation drug carriers and therapeutic agents, particularly in cancer treatment. In this study, the molecular interactions of small fullerene nanoparticles—C20, C22, and C24—with target proteins associated with lung cancer (PDB ID: 1X2J) and breast cancer (PDB ID: 3HY3) were investigated through molecular docking analysis. Each fullerene nanoparticle was docked separately with the specific target protein of the corresponding cancer type, and their binding energies and molecular interaction profiles were compared. The results demonstrated that small fullerenes can form strong and specific interactions with both lung and breast cancer target proteins. These findings suggest that small fullerene nanoparticles hold potential as biological agents or carrier systems in cancer therapy, providing a foundation for future advanced experimental studies. Additionally, HOMO-LUMO contour analyses and Molecular Electrostatic Potential (MEP) maps were visualized and interpreted to evaluate the electronic properties and potential reactive sites of the C20, C22, and C24 complexes.

Keywords: Nanotechnology, Small fullerenes, Molecular docking, Nanoparticle

1. Introduction

Nanotechnology has garnered significant attention in cancer treatment due to its groundbreaking innovations in biomedical applications. Nanoparticles, with sizes ranging from 10 to 100 nanometers [1], offer substantial advantages over conventional treatment methods owing to their high surface area-to-volume ratio and their ability to interact with biomolecules. These dimensional properties enable nanoparticles to be effectively transported within the organism from one organ to another and to deeply penetrate the targeted tissues [1].

Among these advantages are targeted drug delivery, enhanced bioavailability, facilitated intracellular transport, and reduced systemic side effects. Such physical and chemical characteristics impart unique optical and electronic behaviors to nanoparticles, making them indispensable components in the development of advanced diagnostic and therapeutic platforms for cancer detection and treatment [1].

Studies have shown that nanoparticles can improve the targeted delivery of anticancer drugs, reduce systemic toxicity, and enhance therapeutic efficacy [2].

In this context, nanotechnology-assisted approaches hold great promise, particularly in the development of targeted treatment systems and next-generation anticancer agents [3].

Small carbon-based nanostructures such as C20, C22, and C24 exhibit unique physical properties due to their high curvature and distinctly pyramidal carbon atoms [4]. Moreover, these structures are increasingly being considered as novel anticancer agents or drug delivery systems thanks to their exceptional chemical stability, high surface reactivity, and unique behavior in biological environments.

Recent studies have demonstrated that fullerenes possess antioxidant, anticancer, and drug-carrying

[1] Corresponding Authors

e-mail: saadetkaya58@gmail.com

properties, and can be effectively utilized in cellular targeting and controlled drug release systems [5]. Additionally, fullerene derivatives have been reported to inhibit cellular proliferation and slow cancer progression by modulating free radical levels in the tumor microenvironment.

Carbon-based nanostructures, particularly fullerenes, stand out due to their superior chemical and mechanical stability. Small fullerenes (C20, C22, C24), owing to their minimal size and delocalized electron structures, can effectively neutralize reactive oxygen species (ROS), thereby potentially slowing tumor progression associated with oxidative stress [6]. Furthermore, various studies have demonstrated that fullerene derivatives can inhibit cell proliferation [7], activate apoptotic pathways [8], and modulate immune responses within the tumor microenvironment [9].

Specifically, small-sized fullerene nanoparticles such as C20, C22, and C24 are gaining attention for their potential to enhance pharmacokinetic properties and enable precise tumor targeting. These structures can be surface-functionalized to improve biocompatibility and reduce systemic toxicity [9]. It has also been widely reported in the literature that fullerenes can directly interact with biological macromolecules such as DNA, proteins, and cell membranes, and that such interactions can alter cancer cell behavior at the molecular level [10].

In this study, the molecular binding behaviors of the small fullerene nanoparticles C20, C22, and C24 were evaluated through molecular docking analyses with lung cancer target protein (PDB ID: 1X2J) and breast cancer target protein (PDB ID: 3HY3). Additionally, the molecular electrostatic potential (MEP) maps and HOMO–LUMO contour diagrams of C20, C22, and C24 structures were visualized. The aim of this study is to reveal the potential therapeutic effects of these nanoparticles and to provide a scientific foundation for the development of next-generation anticancer agents.

2. Computational Method

The modeling and visualization of the molecular structures of the C20, C22, and C24 complexes were performed using GaussView 6.0.16 software. The molecular geometries of the C20, C22, and C24 compounds were optimized using Density Functional Theory (DFT). All geometry optimizations were successfully completed, and no imaginary frequencies were observed in the systems [4]. For each complex, calculations were performed using the DFT-B3LYP method with the 6-31G basis set. In this context, the B3LYP method represents a hybrid density functional theory (DFT) approach, while 6-31G was chosen as the basis set used in the calculations. Molecular structure visualizations were created using the licensed Chemcraft software [11].

In this study, the 3D structures of the ligand molecules used for molecular docking analyses were downloaded from the PubChem database and subsequently optimized through the DockingServer platform. Energy minimization of the ligands was performed using the MMFF94 force field to obtain appropriate conformations prior to docking [12]. The target protein structures were obtained in pdb format from the Protein Data Bank (PDB) database. Water molecules, non-ligand small molecules, and ions in the protein structures were automatically removed via the DockingServer interface. Missing hydrogen atoms were added, and polar hydrogens were included. Binding interactions between ligands and target proteins were analyzed using virtual screening performed through the DockingServer (www.dockingserver.com) interface. Docking was carried out using AutoDock 4.2, and the Lamarckian Genetic Algorithm (LGA) was employed [13]. After docking, the conformation with the lowest binding energy (kcal/mol) for each ligand was selected for detailed analysis. The obtained ligand-protein complexes were analyzed in terms of hydrogen bonding, Van der Waals, π–π stacking, and hydrophilic/hydrophobic interactions. Visual evaluations and interaction maps were generated using DockingServer's visualization tools and additionally with PyMOL software [14].

3. Results and discussion

The C20, C22, and C24 structures presented in Figure 1 were obtained using the B3LYP/6-31G hybrid functional [15]. It was observed that each structure reached a stable conformation, supported by bond lengths obtained during energy minimization and symmetric arrangements in the ring structures. Notably, the C20 structure stands out with its high spherical symmetry, while the C22

and C24 species exhibit more complex and extended skeletal frameworks.

3.2. Molecular Electrostatic Potential (MEP) Analysis

Molecular electrostatic potential (MEP) is an effective theoretical analysis method that shows how electrostatic forces are distributed in three-dimensional space around a molecule. MEP is highly important for identifying intermolecular interaction sites and detailing reactive regions [16]. In this study, the electrostatic potential distributions of the C20, C22, and C24 carbon cage structures were calculated using the Gaussian16 program based on geometries optimized with the DFT-based B3LYP functional and 6-31G basis set, and the obtained results were visually analyzed. Determining the electrostatic properties on these structures enabled a clearer identification of potential interaction sites on molecular surfaces.

In the electrostatic potential maps, the potential distribution is represented by colors ranging from most negative to most positive as red, yellow, green, light blue, and dark blue, respectively [17]. Blue indicates regions with highly positive electrostatic potential, red indicates areas with highly negative electrostatic potential, and green indicates regions with zero potential [18].

Regions with positive electrostatic potential (blue) are considered nucleophilic interaction sites, while regions concentrated with negative potential (red) stand out as reactive sites targeted by electrophilic species [19]. The calculated MEP maps for the C20, C22, and C24 structures are presented in Figure 2.

Figure 1. Optimized geometric structures of C20, C22, and C24 complexes.

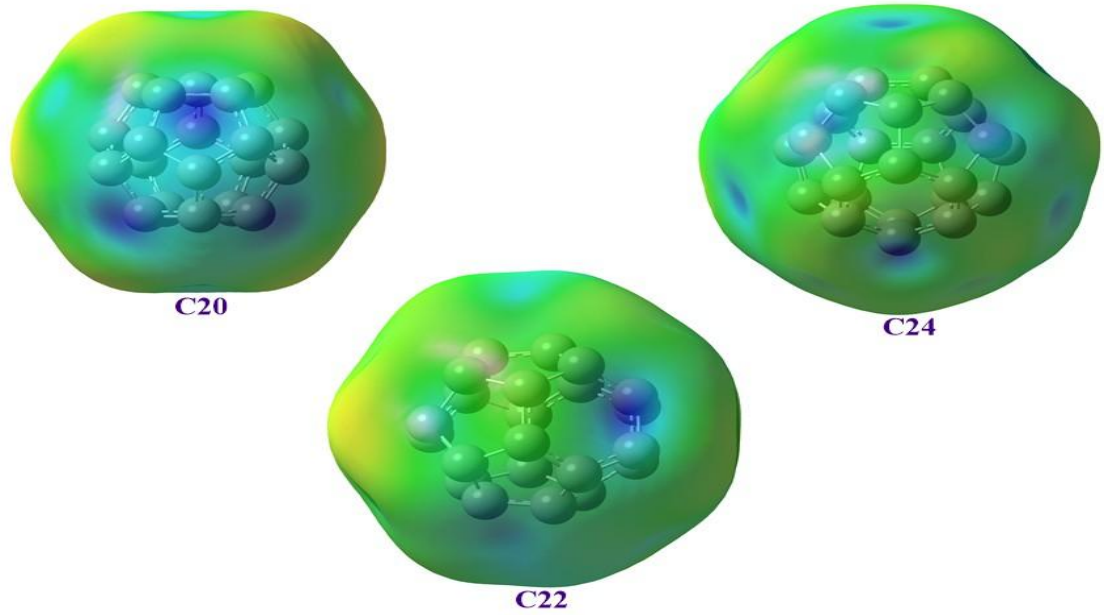

Figure 2. Molecular Electrostatic Potential (MEP) maps of the C20, C22, and C24 structures.

The prominent dark blue regions in the C20 structure indicate a higher positive electrostatic potential density on some surfaces of this molecule, suggesting a greater tendency to interact with nucleophilic species. In contrast, the predominantly green tones and more balanced color distribution

observed in the MEP maps of the C22 and C24 structures indicate a more uniform charge distribution on their surfaces, reflecting a more electrostatically neutral character. Additionally, the absence of red regions in the C20, C22, and C24 structures suggests that these molecules may be reactive toward electrophilic attacks. In this context, it can be interpreted that as the molecular size increases, the differences in surface potential decrease and electrostatic symmetry becomes more pronounced.

3.3. Frontier Molecular Orbital Analyses

The Highest Occupied Molecular Orbital (HOMO), which is the highest energy filled orbital, and the Lowest Unoccupied Molecular Orbital (LUMO), which is the lowest energy empty orbital, are critical for understanding a molecule's chemical reactivity, stability, and electronic properties. HOMO represents the molecule's ability to donate electrons, while LUMO represents its ability to accept electrons [20]. The energy gap between these two orbitals, known as the HOMO–LUMO energy gap (E_{gap}), is an important parameter that determines the molecule's electronic transitions, optical properties, and chemical stability.

One of the key parameters in describing a molecule's electronic behavior is the energy difference (ΔE) between the HOMO and LUMO, defined by the following equation:

$$\Delta E = E_{LUMO} - E_{HOMO} \qquad \text{Equation 1.}$$

This expression represents the difference between the energy level of the Lowest Unoccupied Molecular Orbital (LUMO) and the energy level of the Highest Occupied Molecular Orbital (HOMO) [20].

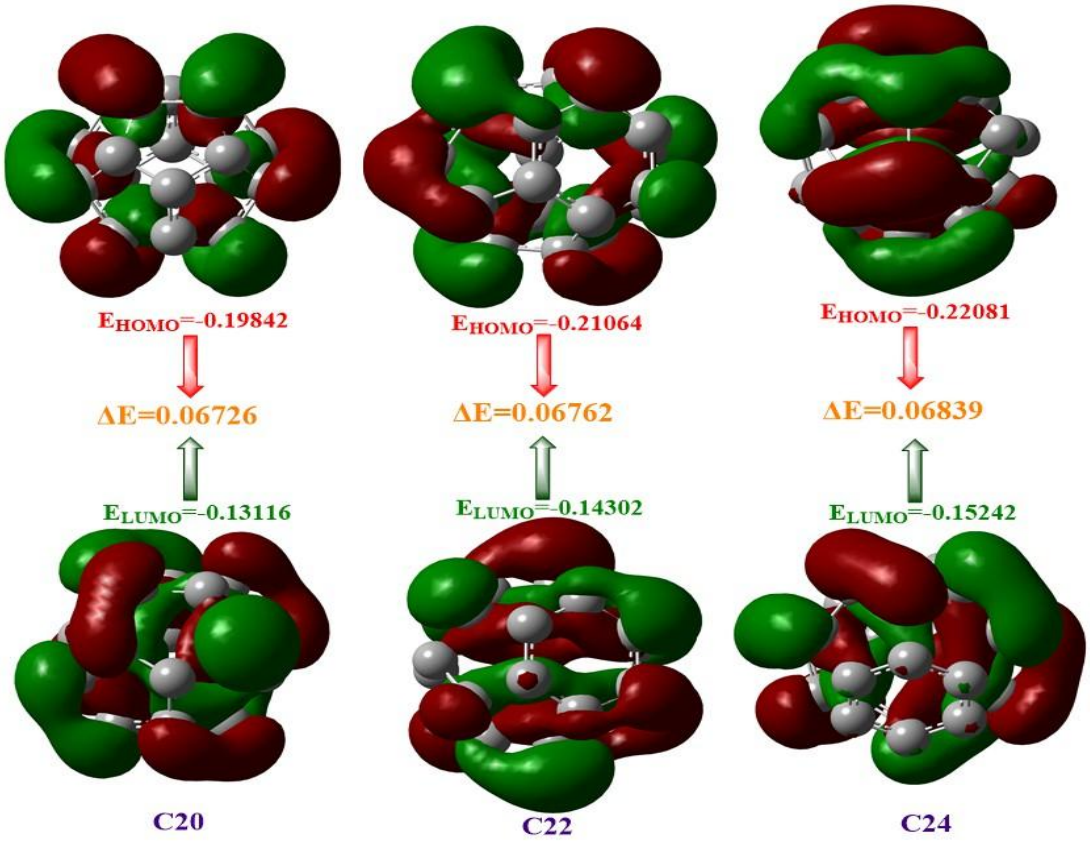

Figure 3. HOMO-LUMO diagrams of the C20, C22, and C24 structures.

The frontier molecular orbital (FMO) visualizations of the C20, C22, and C24 molecules shown in Figure 3 allow for a comparative evaluation of the electronic properties of these structures. When examining the HOMOs of the structures, it is observed that the orbital density in C20 is localized

in certain regions, whereas in C22 and especially in C24, this distribution exhibits a more widespread character. This suggests that π-electron delocalization increases with structural size and that symmetry is reflected in the electronic structure.

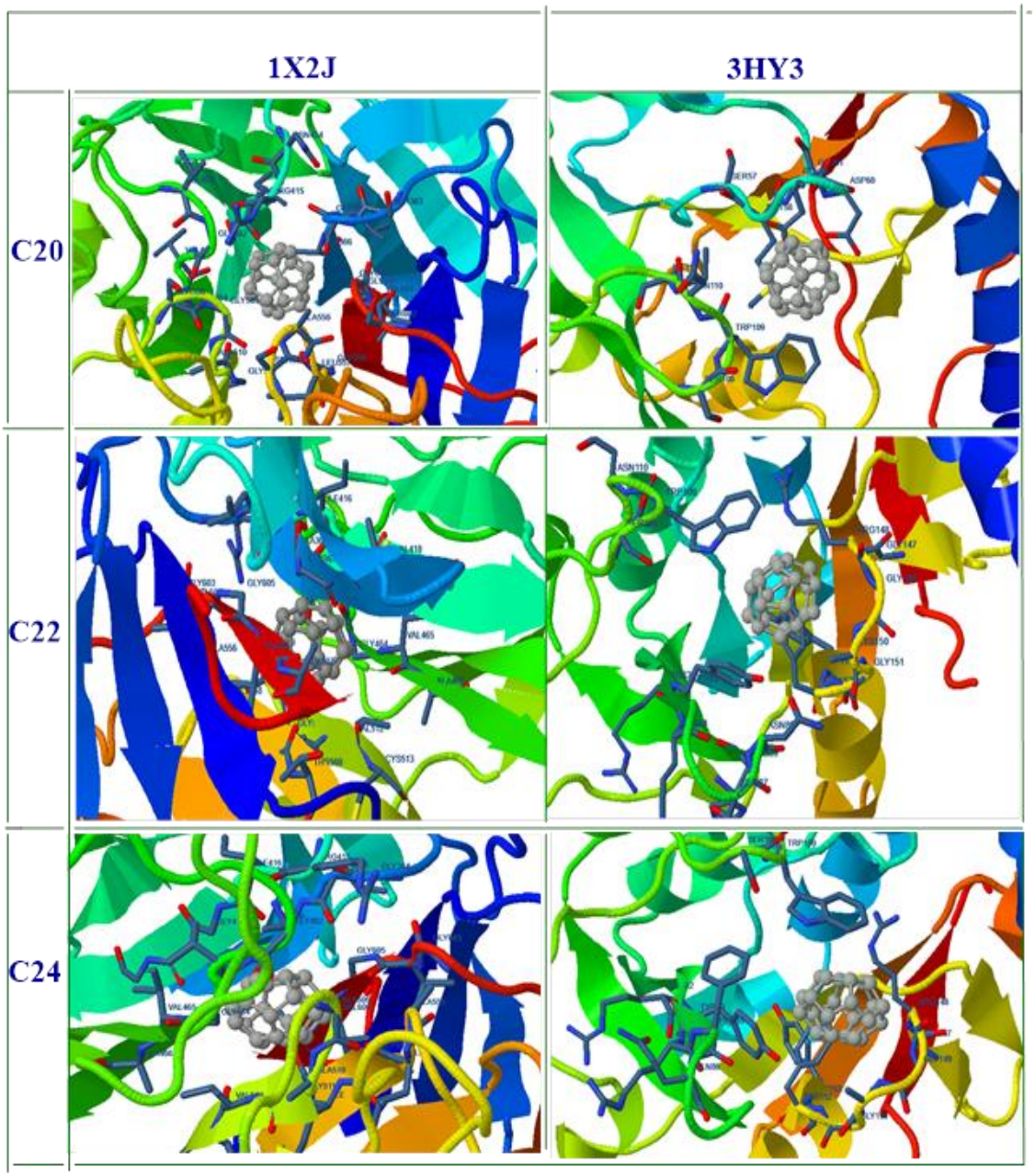

Figure 4. Binding modes of small fullerenes with target proteins 1X2J and 3HY3.

In terms of energy levels, the HOMO energies were calculated as -0.19842 eV for C20, -0.21064 eV for C22, and -0.22081 eV for C24, respectively. The shift of the HOMO level toward more negative values indicates that increased structural complexity leads to a more stable electron distribution and that the molecular system has a lower tendency to donate electrons. Similarly, the LUMO levels are 0.13116 eV for C20, 0.14302 eV for C22, and 0.15242 eV for C24, showing an increasing trend with structural size. This increase implies a higher energy requirement for electron acceptance and suggests that the structures may be less sensitive to electron transfer reactions.

The energy gap (ΔE) between HOMO and LUMO is one of the fundamental parameters that directly affect a molecule's chemical behavior and electronic stability. The smaller the ΔE value, the softer the molecule is considered and the greater its tendency to participate in chemical reactions;

conversely, higher ΔE values indicate that the system is more stable and kinetically inert [21].
In this context, the ΔE values were calculated as 0.06726 eV for C20, 0.06762 eV for C22, and 0.06839 eV for C24. This gradual increase in ΔE values suggests that chemical stability is higher and reactivity is lower, especially for the C24 structure. These results demonstrate that the electronic properties of these structures can be finely tuned depending on their size, and such systems may exhibit adjustable properties in optoelectronic applications.

3.4. Molecular Docking

Molecular docking is a powerful computational technique used to predict the binding mode and affinity between a ligand and a target protein. This method is widely employed, especially in drug design and the molecular-level understanding of biological targets [22]. Through docking analyses, it is possible to determine how the ligand binds to the protein, which amino acid residues it interacts with at the binding site, and thermodynamic parameters such as binding energy [23]. The molecular binding modes of C20, C22, and C24 nanoparticles with the lung cancer target protein PDB ID=1X2J and the breast cancer target protein PDB ID=3HY3 are presented in Figure 4.
In this study, the interaction potentials of C20, C22, and C24 carbon structures with lung cancer (1X2J) and breast cancer (3HY3-MCF7) target proteins were analyzed in detail using molecular docking. As a result of the analyses, the binding energy, inhibitor concentration (Ki), types of intermolecular interactions, and interaction surfaces of each molecule were calculated. The obtained results revealed noticeable differences in the strength of interactions these structures exhibited with biological targets. Among the calculations, the strongest binding energy of -11.55 kcal/mol was observed for the interaction of the C24 molecule with the lung cancer target. The calculated molecular docking table of the C20, C22, and C24 structures is presented in Table 1. and Table2.

Table 1. Docking results of C20, C22, and C24 against PDB ID=1X2J

Property	**C20**	**C22**	**C24**
$\Delta G_{binding}$ (kcal/mol)	-8.57	-9.98	-11.55
Ki	523.95 nM	48.05 nM	3.41 nM
vdW+HB+desolv (kcal/mol)	-8.57	-9.98	-11.54
Total Intermolecular (kcal/mol)	-8.57	-9.98	-11.55
Interaction Surface	499.348	532.581	546.878

Table 2. Docking results of C20, C22, and C24 against PDB ID=3HY3

Property	**C20**	**C22**	**C24**
$\Delta G_{binding}$ (kcal/mol)	-4.49	-5.90	-6.50
Ki	510.45 µM	47.58 µM	17.12 µM
vdW+HB+desolv (kcal/mol)	-4.49	-5.90	-6.51
Total Intermolecular (kcal/mol)	-4.49	-5.90	-6.50
Interaction Surface	381.115	584.636	584.932

The highest binding affinity was recorded for the interaction of the C24 molecule with the 1X2J target protein, with a binding energy of -11.55 kcal/mol and an estimated inhibitor concentration of only 3.41 nM, making this molecule stand out as the strongest candidate by far. The C22 molecule also demonstrated a strong binding profile, showing a notable effect with -9.98 kcal/mol and a Ki value of 48.05 nM. In contrast, the C20 binding energy to the same target was -8.57 kcal/mol, indicating a lower binding capacity.
When examining the types of interactions, it was observed that hydrophobic contacts dominated and that binding conformations were stabilized by these interactions. Notably, the C24 structure was found to form intense π–π stacking interactions with aromatic amino acids such as TYR152, TYR83, and TRP109. These types of interactions help the ligand fit snugly into the active site, creating a more

stable complex [25]. Similarly, the C22 molecule achieved a highly favorable position in the binding site through hydrophobic contacts with ALA366 and ILE559.

In the docking analyses, electrostatic contributions were mostly negligible, with the total binding energies largely driven by Van der Waals and hydrophobic forces. Therefore, ligands tended to interact with apolar surface regions, and conformational fit was seen as more decisive than electrostatic attraction [26].

Overall, it was concluded that as the size of the structure increased, the interaction surface expanded, which in turn enhanced binding affinity. Specifically, the C24 molecule maximized binding stability by contacting a greater number of amino acid residues due to its large surface area. For this reason, C24-derived fullerene structures should be considered potential inhibitors for lung cancer target proteins, and these structures should be supported with advanced in vitro and in silico studies to be integrated into drug development processes.

4. Conclusions

C20, C22, and C24 structures have been comprehensively investigated through quantum chemical calculations focusing on their geometric optimizations, electronic structure analyses, and biological interaction potentials. The calculations were performed at the DFT-B3LYP/6-31G level. The HOMO–LUMO analyses obtained in this study provide crucial insights into the electronic properties of these structures. The distribution of orbital densities on the molecular surfaces shows an increasing delocalization with the growth in size, indicating that the π-electrons spread over larger areas as the cage expands.

When comparing energy levels, the C24 structure exhibits a higher energy gap (ΔE = 0.06839 eV) between its EHOMO (-0.22081 eV) and ELUMO (0.15242 eV) values compared to C20 and C22. This suggests that C24 possesses a more stable electronic structure with lower excitability. Overall, as the molecular size increases, the HOMO-LUMO energy gap widens and the orbitals become more delocalized. This implies that larger carbon cages enhance electronic stability and thus may be preferred in optoelectronic applications.

Analyses based on Molecular Electrostatic Potential (MEP) maps reveal that the electrostatic distribution on the surfaces of C20, C22, and C24 varies according to their structural size. In C20, prominent dark blue regions represent localized positive potential areas, indicating sites that may be prone to interactions with nucleophilic species. Conversely, the MEP maps of C22 and C24 show a more homogeneous color distribution dominated by green shades, reflecting a more balanced and neutral surface potential. The limited presence of red tones points to low negative electrostatic potential, suggesting these structures are less reactive toward electrophilic species. With increasing size, the surface electrostatic charges are observed to distribute more symmetrically and evenly, demonstrating that larger carbon cages restrict reactive sites, resulting in more stable and orderly electronic architectures.

Docking results with the breast cancer target protein 3HY3 revealed weaker binding energies compared to the lung cancer protein. In this context, C24, C22, and C20 exhibited binding energies of -6.50, -5.90, and -4.49 kcal/mol, respectively. Therefore, fullerene-like carbon structures appear to show a more selective and stronger binding tendency particularly towards lung cancer targets [22, 24].

References

[1] N. Alrushaid, F. A. Khan, E. A. Al-Suhaimi, & Elaissari, A. Nanotechnology in cancer diagnosis and treatment. Pharmaceutics, , 15(3), (2023) 1025.

[2] K. Elumalai, S. Srinivasan, & A. Shanmugam Review of the efficacy of nanoparticle-based drug delivery systems for cancer treatment. Biomedical Technology, 5, (2024) 109-122.

[3] D. Bobo, K. J. Robinson, J. Islam, K. J. Thurecht, & S. R. Corrie. Nanoparticle-based medicines: A review of FDA-approved materials and clinical trials to date. Pharmaceutical Research, 33(10), (2016) , 2373–2387.

[4] N. Kosar, H. Tahir, K. Ayub, & T. Mahmood. DFT studies of single and multiple alkali metals doped C24 fullerene for electronics and nonlinear optical applications. Journal of Molecular Graphics and Modelling 105, (2021), 107867.

[5] N. B. Fernandes, R. U. K. Shenoy, K M. K. ajampady, C. E. DCruz, R. K. Shirodkar, L. Kumar, & R. Verma. Fullerenes for the treatment of cancer: an emerging tool. Environmental Science and Pollution Research 29(39), (2022) 58607-58627.

[6] R. Bakry, R. M. Vallant, M. Najam-ul-Haq, M. Rainer, Z. Szabo, C. W. Huck, & G. K. Bonn. Medicinal applications of fullerenes. International Journal of Nanomedicine 2(4), (2007) 639–649.

[7] M. Krause, et al. Fullerene–biomolecule interactions: Understanding the potential for nanomedicine. ChemBioChem 19(1), (2018) 1–10.

[8] X. Zhao, et al. Fullerene nanomaterials inhibit cancer progression by regulating oxidative stress and apoptosis pathways. Nanomedicine 14(4), (2019) 451–464.

[9] G. V. Andrievsky, M. V. Kosevich, O. M. Vovk, V. S. Shelkovsky, & L. A. Vashchenko. Studies of aqueous colloidal solutions of fullerene C60 by electron microscopy. Chemical Physics Letters 364(1–2), (2002) 8–17.

[10] H. Yamawaki, & Y. Imai. Potential toxicity of engineered nanoparticles in the lung. Advanced Drug Delivery Reviews, 58 (14) (2006) 1436–1441.

[11] S. Erkan & D Karakaş. DFT investigation and molecular docking studies on dinuclear metal carbonyls containing pyridyl ligands with alkyne unit. Chemical Papers 73, (2019) 2387-2398.

[12] Z. Bikadi & E. Hazai. Application of the PM6 semi-empirical method to modeling proteins enhances docking accuracy of AutoDock. Journal of cheminformatics 1, (2009) 1-16.

[13] R. Huey, G. M. Morris, A. J. Olson, & D. S. Goodsell. semiempirical free energy force field with charge-based desolvation. Journal of computational chemistry 28(6), (2007) 1145-1152.

[14] J. J. Stewart Stewart computational chemistry. (2007) http://openmopac. net/

[15] Frisch, M. J. E. A. gaussian 09, Revision d. 01, Gaussian. Inc, Wallingford CT (2009) 201.

[16] P. Politzer & J. S. Murray. The fundamental nature and role of the electrostatic potential in atoms and molecules. Theoretical Chemistry Accounts 108(3), (2002) 134-142.

[17] A. M. Bayoumy, M. Ibrahim & A.Omar. Mapping molecular electrostatic potential (MESP) for fulleropyrrolidine and its derivatives. Optical and Quantum Electronics 52, (2020) 1-13.

[18] Z. Akbari, C. Stagno, N. Iraci, T. Efferth, E. A. Omer, A. Piperno,... & N. Micale Biological evaluation, DFT, MEP, HOMO-LUMO analysis and ensemble docking studies of Zn (II) complexes of bidentate and tetradentate Schiff base ligands as antileukemia agents. Journal of Molecular Structure 1301, (2024) 137400.

[19] S. Zinatloo-Ajabshir, S. Rakhshani, Z. Mehrabadi, M. Farsadrooh, M. Feizi-Dehnayebi, S. Rakhshani,... & T. M. Aminabhavi. Novel rod-like [Cu (phen) 2 (OAc)]· PF6 complex for high-performance visible-light-driven photocatalytic degradation of hazardous organic dyes: DFT approach, Hirshfeld and fingerprint plot analysis. Journal of Environmental Management 350, (2024) 119545.

[20] R. G. Parr Density functional theory of atoms and molecules. In Horizons of Quantum Chemistry: Proceedings of the Third International Congress of Quantum Chemistry Held at Kyoto, Japan, October 29-November 3, 1979 , (1989) (pp. 5-15).

[21] R. G. Pearson. Absolute electronegativity and hardness: application to organic chemistry. Journal of Organic Chemistry 54(6), (1986) 1423–1430

[22] X. Y. Meng, H. X. Zhang, M. Mezei, & M. Cui. Molecular docking: a powerful approach for structure-based drug discovery. Current computer-aided drug design 7(2), (2011) 146-157.

[23] G. M. Morris, R. Huey, W. Lindstrom, M. F. Sanner, R. K. Belew, D. S. Goodsell, & A. J. Olson. AutoDock4 and AutoDockTools4: Automated docking with selective receptor flexibility. Journal of computational chemistry 30(16), (2009) 2785-2791.

[24] D. B. Kitchen, H. Decornez, J. R. Furr & J. Bajorath. Docking and scoring in virtual screening for drug discovery: methods and applications. Nature Reviews Drug Discovery 3(11), (2004) 935–949.

[25] S. Y. Huang, S. Z. Grinter, & X. Zou. Scoring functions and their evaluation methods for protein–ligand docking: recent advances and future directions. Physical Chemistry Chemical Physics 12(40), (2010) 12899–12908.

[26] N. S. Pagadala, K. Syed, & J. Tuszynski. Software for molecular docking: a review. Biophysical Reviews 9(2), (2017) 91–102.